THE JOURNAL OF PHYSICAL CHEMISTRY LETTERS
A JOURNAL OF THE AMERICAN CHEMICAL SOCIETY

pubs.acs.org/JPCL

Letter

Link between Gas Phase Reaction Chemistry and the Electronic Conductivity of Atomic Layer Deposited Titanium Oxide Thin Films

Aein S. Babadi, Robert Tang-Kong, and Paul C. McIntyre*

Cite This: *J. Phys. Chem. Lett.* 2021, 12, 3625−3632

Read Online

ACCESS | Metrics & More | Article Recommendations | Supporting Information

ABSTRACT: In situ monitoring of gas phase composition reveals the link between the changing gas phase chemistry during atomic layer deposition (ALD) half-cycle reactions and the electronic conductivity of ALD-TiO_2 thin films. Dimethylamine ($(CH_3)_2NH$, DMA) is probed as the main product of both the TDMAT and water vapor half-reactions during the TDMAT/H_2O ALD process. In-plane electronic transport characterization of the ALD grown films demonstrates that the presence of DMA, a reducing agent, in the ALD chamber throughout each half-cycle is correlated with both an increase in the films' electronic conductivity, and observation of titanium in the 3+ oxidation state by ex situ X-ray photoelectron spectroscopy analysis of the films. DMA annealing of as-grown TiO_2 films in the ALD chamber produces a similar effect on their electronic characteristics, indicating the importance of DMA-induced oxygen deficiency of ALD-TiO_2 in dictating the electronic conductivity of as-grown films.

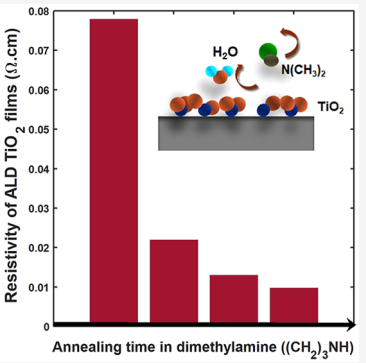

Atomic layer deposition (ALD) is a cyclic form of chemical vapor deposition enabling growth of highly uniform and conformal thin films over complex surface topologies for many applications including electronics and energy technologies. For example, ALD has become an indispensable tool in nanoelectronics to form the gate dielectric layers at the heart of metal oxide semiconductor field effect transistors.[1,2] The availability of a large range of molecular precursors enables development of ALD processes for deposition of a wide array of metal oxides, nitrides, phosphides, sulfides, carbides, and an increasing number of elemental metals. ALD has become increasingly important in corrosion protection,[3,4] synthesis of catalysts,[5,6] battery electrode coatings,[7−9] and in surface passivation of solar cells.[10−14]

Atomic layer deposited titanium dioxide (ALD-TiO_2) is a widely studied transition metal oxide thin film material, in part because of its chemical stability and its technologically important optical and electronic properties. Titanium oxide is a photocatalyst that activates photoinduced decomposition of organic contaminants so that TiO_2 coatings can produce "self-cleaning" surfaces.[15−17] Furthermore, TiO_2 thin films also function as electron-selective contacts for optoelectronic devices including solar cells.[18−21] Atomic layer deposited TiO_2 also serves as a barrier to oxidative corrosion of underlying efficient semiconductor light absorbers in aqueous electrolytes,[3,22] enabling stable water splitting for solar fuel synthesis. These varied and significant applications of thin TiO_2 films provide motivation for understanding the relationships among ALD synthesis conditions and the physical and chemical properties of atomic layer deposited TiO_2.

A commonly used ALD chemistry for TiO_2 deposition involves introducing alternating pulses of the precursor tetrakis(dimethylamido)titanium (TDMAT) and of water vapor into a reaction chamber at a pressure in the 100s of mTorr to Torr range. The half-cycle reactions in this process are conceptually simple (Figure 1). However, the parameter space for synthesis of the TiO_2 product can be enormous. Determining the influence of the input reactant activities, temperature, pressure, and other variables on the composition and structures of the film is a highly complex multifactorial problem.

Scheuermann et al. studied amorphous as-deposited ALD-TiO_2 films in the thickness range of 1−10 nm deposited at substrate temperature of 170 °C on p^+Si coated with a ∼1.3 nm thick chemically derived SiO_2 layer. Current versus potential curves were collected for every sample in the thickness series in aqueous solution in a photoelectrochemical cell. It was discovered that the resulting, amorphous, TiO_2 samples exhibited an ohmic resistance corresponding to an additional overpotential of ∼21 mV per nm of film thickness to support 1 mA/cm^2 of electron current flowing from a top Ir catalyst layer to an underlying p+Si substrate, for TiO_2 film thicknesses greater than ∼2 nm.[23] This behavior was attributed to a polaronic hopping conduction mechanism for electrons injected into the TiO_2, consistent with the reported energies of Ti^{3+} electronic states[24] well-aligned with valence band edge of

Received: January 11, 2021
Accepted: March 5, 2021

https://doi.org/10.1021/acs.jpclett.1c00115
J. Phys. Chem. Lett. 2021, 12, 3625−3632

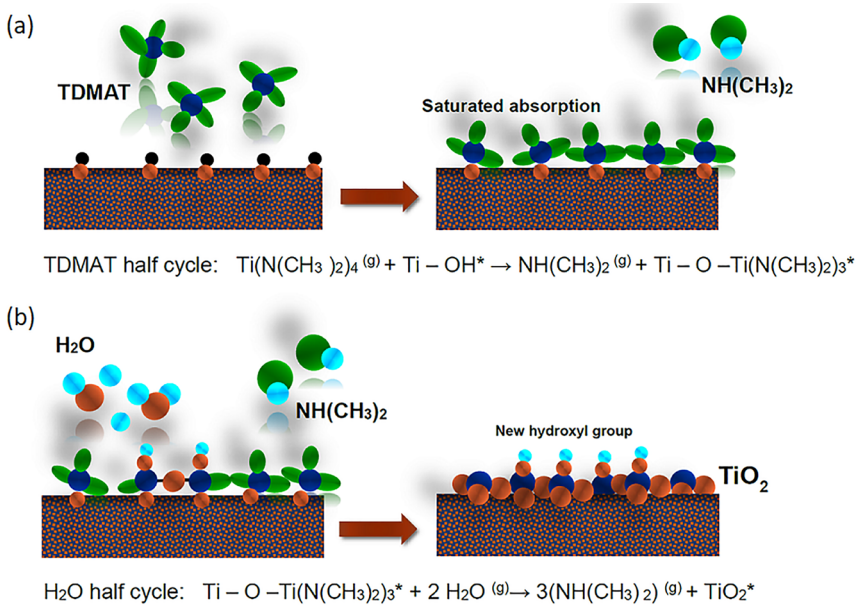

Figure 1. Representation of the ALD process using TDMAT and water as precursors to deposit TiO_2. (a) Half cycle reaction of TDMAT with hydroxyl sites on already TiO_2 covered surface and (b) reaction of H_2O molecules with the remaining dimethylamido groups, which depicts the hydroxylation process and development of Ti−O−Ti bridge bonding in the deposited film. After completion of the cycle a layer of TiO_2 film is formed on the surface in which, ideally, all of Ti atoms are connected to each other by oxygen atoms. The asterisks (∗) designate the surface species.

silicon and the work function of Ir. The results reported in ref 23 differ from those later reported by Hu et al.[25] that imply an almost thickness-independent resistance for ALD-TiO_2 coated Si photoanodes in a water splitting cell for film thicknesses in the range 4−143 nm. Both studies used the TDMAT/H_2O ALD chemistry with similar chamber pressure, substrate, and source temperatures, although the reactor designs were different.

The wide variance of the reported electronic conductivity of as-deposited amorphous ALD-TiO_2 films grown under nominally very similar conditions suggests significant chamber-to-chamber differences in the transient gas phase reaction chemistry of this ALD process. The influence of reaction intermediates and gas phase reaction products on the stoichiometry and the important physical and chemical properties of ALD-grown metal oxide layers has received little attention to date. In the case of the TDMAT/H_2O ALD chemistry, dimethylamine (DMA; $(CH_3)_2NH$) is an expected product of both the TDMAT and water vapor half-reactions. Adsorption of DMA, in the presence of a high coverage of surface oxygen, has been studied as early as 1970s,[26] and the reported results indicate that DMA can act as potent reducing agent. Therefore, the DMA reaction product of the TDMAT/H_2O chemistry has the potential to induce oxygen deficiency of a growing TiO_2 film transiently, by, for example, its reaction with surface oxygen-containing species, if it is not efficiently removed from the reactor during the ALD process. Reduction of TiO_2 results in the formation of oxygen vacancies. Titanium ions are in excess with respect to oxygen ions, and the reduction of TiO_2 is accompanied by the appearance of Ti^{3+} species. For sufficiently large oxygen vacancy concentrations, nanoscale TiO_{2-x} can exhibit band gap narrowing and a high density of donor-type oxygen vacancy states near the titanium oxide conduction band edge, enhancing its electronic conductivity.[27,28]

Herein, we describe an experimental study to test the hypothesis that dimethylamine exposure reduces the TiO_2 film and thus enhances the electrical conductivity by introducing oxygen deficiency. Residual gas analysis during ALD was used to probe the dynamics of DMA formation and removal during each reaction cycle, and the purge duration was varied to alter the fraction of process time during which a growing TiO_2 film was exposed to DMA. Altering the purge duration during TiO_2 atomic layer deposition changes several physical properties of the films that may affect electronic conductivity distinct from the influence of oxygen stoichiometry. Therefore, intentional exposure of ALD-grown films to DMA during postgrowth annealing in the ALD chamber at the ALD substrate temperature and pressure was investigated as a means of controlled DMA exposure. The results obtained demonstrate that DMA exposure significantly increases the electrical conductivity of TiO_2 thin films and that this change coincides with the observation of Ti^{3+} ions by X-ray photoelectron spectroscopy, supporting the hypothesis of in situ reduction of the films by DMA.

Experiments were performed in a custom-designed ALD system with a load lock to ensure a low base pressure (~1×10^{-6} Torr) for the process chamber with the aim of minimizing the potential wall reaction/contamination during wafer loading and unloading. A residual gas analyzer (RGA) with the mass range of 1−300 amu was installed in the ALD reactor to acquire real-time chemical diagnostic data of the TiO_2 ALD process. An adequate pressure gradient between the process environment (0.4 Torr) and the RGA region (1×10^{-6} Torr) was maintained through a differentially pumped sampling system. TiO_2 films were grown at a substrate temperature of 175 °C using half-cycle dosing of tetrakis(dimethylamino)-titanium (TDMAT) and water vapor on both p-type silicon single crystal substrates with resistivity of 0.001−0.005 Ω·cm and fused silica. The silicon substrate samples were used for physical characterization while all the electrical measurements

https://doi.org/10.1021/acs.jpclett.1c00115
J. Phys. Chem. Lett. 2021, 12, 3625−3632

were performed on the fused silica samples with higher substrate resistivity on the order of 10^{17} Ω·cm.

The deposition began with a TDMAT pulse and then proceeded to a water vapor pulse, with evacuation and nitrogen purging steps in between each pulse. The temperature of the liquid TDMAT and H_2O sources are 80 and 50 °C, respectively. Reported vapor pressure data are consistent with vapor pressures of 3.31 and 92.5 Torr above the TDMAT and H_2O sources, respectively. The TDMAT and water pulse times were both 3 s, giving an estimated dose into the chamber of 9.4 Torr·s for TDMAT and 278 Torr·s for water vapor per ALD cycle. This greatly exceeds the saturation dose required for monolayer adsorption on the growing film surface. For example, assuming an approximate saturation coverage of 2.5×10^{18} m^{-2} for TDMAT molecules,[29] the saturation dose of TDMAT is estimated to be ~2.2 L or 2.2×10^{-6} Torr·s. The nitrogen purge pressure was kept at approximately 0.4 Torr during precursor pulsing intervals of 120 s. TiO_2 films were prepared using 240 ALD cycles, giving a nominal thickness of ~10 nm. The film thickness was measured by ellipsometry, and further confirmed by X-ray reflectivity (XRR). In a subset of the experiments, TiO_2 films were in situ annealed in the ALD chamber at the end of the depositions and at the same substrate temperature used for deposition, 175 °C. Anneals were performed in a dimethylamine ambient for 15 to 60 min duration. The chamber was evacuated before the DMA was introduced at 1 sccm at a base pressure of ~1−2 mTorr. Then the chamber was purged and cooled down in N_2 flow of 100 sccm.

Grazing incidence X-ray diffraction (GIXRD) analysis revealed that all TiO_2 films, both DMA-annealed and unannealed, are largely amorphous, with sporadic detection of weak anatase phase diffraction peaks that are attributed to small number of crystallites in an amorphous matrix. As-deposited and thin TiO_2 films are expected to be amorphous. Nanocrystalline anatase phase has been reported in TiO_2 films >7 nm in thickness after annealing at temperatures exceeding 300 °C, significantly higher than the DMA anneal temperature used in the present experiments.[23] Electrical conductivity of TiO_2 films deposited on highly resistive fused silica substrates was measured using the transmission line method (TLM). Linear TLM test patterns with dimensions of 50 μm × 30 μm were defined by electron beam evaporation of Pt electrodes (200 nm thickness) onto the TiO_2-coated substrates through a shadow mask.

Real-time residual gas analysis was used to provide a link between changes in gas phase chemistry during ALD half-cycle reactions and the properties of the deposited films. Half reactions occur such that a partial monolayer of precursor, for example, TDMAT, forms by chemisorption at reactive sites on the substrate until these sites are saturated. Intermediate steps of inert gas purging and evacuation clears the chamber of excess first precursor and then the second precursor pulse, for example, of water vapor, is introduced, followed by another purge step to complete the deposition cycle.

Figure 2 shows the transient sampling of gas phase species by residual gas analysis during successive TDMAT and H_2O ALD pulses on TiO_2 surface at 175 °C. The partial pressures of the gas phase species were collected after 15 cycles of TiO_2 ALD on Si substrates. Excess precursor and reaction byproducts were purged with a constant flow of N_2 gas for 120 s. The purge segments result in a gradual decrease of the respective RGA signal to noise levels. A dimethylamine

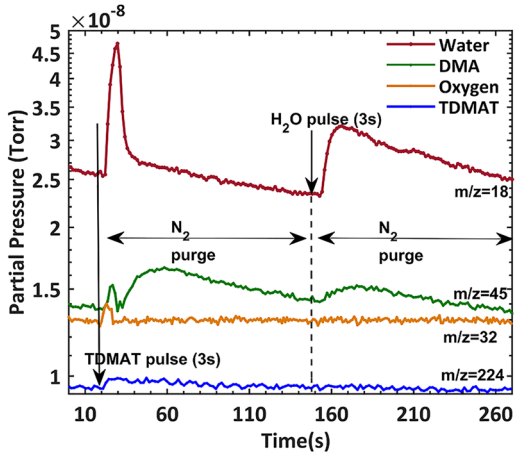

Figure 2. Transient sampling of gas phase species by residual gas analysis during the TDMAT and H_2O ALD process at 175 °C. Excess precursor molecules and reaction byproducts are purged with constant flow of N_2 gas for 120 s. Subsequent purges result in a rapid decrease of their respective RGA signal-to-noise levels.

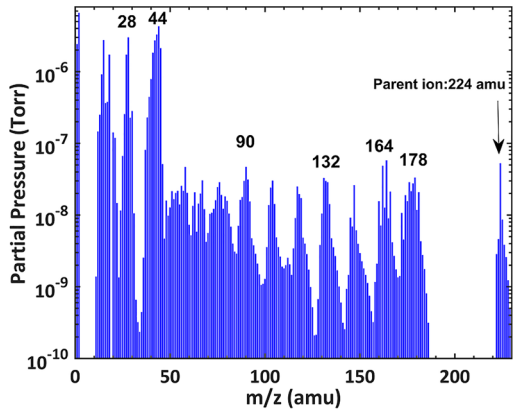

Figure 3. Mass spectrum of TDMAT showing the molecular parent ion at m/z = 224 amu and the electron impact ionization cracking pattern.

($(CH_3)_2NH$) signal is detected in the chamber gas ambient throughout each ALD cycle. Figure 3 displays a typical mass spectrum with TDMAT, sampled at 175 °C the deposition temperature of TiO_2 films. The molecular parent ion is clearly observed at m/e = 224 amu and DMA ($(CH_3)_2NH$) at 45 amu. The 44 amu fragment is associated with $N(CH_3)_2$ and may originate from the reaction of the ligands on TDMAT with oxygen-containing species in the reactor or, possibly, from TDMAT thermal decomposition products.[30] One possible pathway for oxygen and DMA reaction proceeds by removing a hydrogen atom from DMA to form OH and $N(CH_3)_2$.[31] The fragmentation pathways expected for $C_2H_6N^+$ ions can produce NH_4 and CH_4.[32] Although these masses are detectable by RGA, they have overlapping peak patterns with water for primary peaks at 16, 17, and 18 related to O^+, HO^+, and H_2O^+ species. The heavier species (90, 132, 164, and 178 amu) labeled on the spectrum are attributed fragments of undecomposed TDMAT molecules or products of the TDMAT decomposition and the reaction intermediates. Peaks from fragments of undecomposed TDMAT may overlap with many of the peaks from decomposition products and their fragments. This makes it difficult to conclusively determine

https://doi.org/10.1021/acs.jpclett.1c00115
J. Phys. Chem. Lett. 2021, 12, 3625−3632

whether the detected species were formed in the reactor or in the ionizer.

Figure 4 shows transient sampling of gas phase species with constant flow of N_2 gas for 300 s. With a longer nitrogen purge,

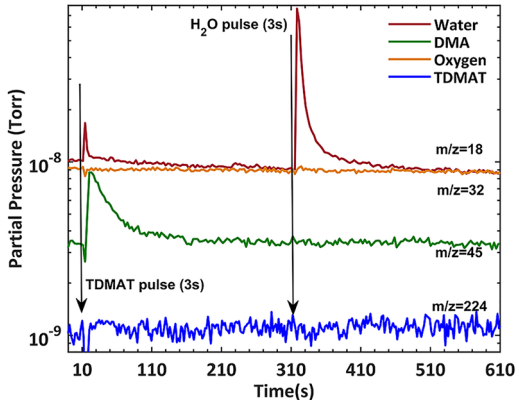

Figure 4. Transient sampling of gas phase species by residual gas analysis during the TDMAT and H_2O ALD pulses, while excess precursors and reaction byproducts are purged with constant flow of N_2 gas for 300 s.

the dimethylamine byproduct signal is reduced to the RGA background level before the H_2O pulse occurs. Not detecting a distinct rise in the m/e = 45 signal after the H_2O pulse suggests there is less unreacted DMA and TDMAT fragment of 45 amu in the chamber during the second half ALD cycle. The 44 amu fragment of DMA, ($N(CH_3)_2$) signal, was however measurable during both water and TDMAT half cycle reactions (Supporting Information, Figure S2). The detection of the signal could also be limited by the RGA response time, which increases with the number of mass-charge values that are simultaneously measured and is influenced by the partial pressure levels. The response of the RGA was 3.07 s for the spectra in Figure 4, which is slightly longer than the H_2O pulse time duration. This may limit detection of the m/e = 45 signal after the H_2O pulse (Supporting Information, Figure S3). The XRR analysis of the TiO_2 films depicted a decrease in the thickness of the as-deposited TiO_2 film from 10.1 to 7.85 nm and an increase in the film density from 3.6 to 4.58 g/cm^3 with an increase in purging time from 120 to 300 s (Supporting Information, Figures S4 and S5). For increasing purge duration, the growth per cycle is reduced due to precursor desorption after each TDMAT pulse and by dehydration of the metal oxide film surface after each H_2O pulse.[33] The reduced growth per cycle will coincide with increased film density if surface restructuring and removal of trapped reaction intermediates are also affected by the longer purge time.

Figure 5 shows the measured average in-plane resistance of the deposited TiO_2 films as a function of TLM pad spacing for different ALD conditions. TLM measurements detect a dramatic increase in the resistivity of the TiO_2 films deposited with longer purge intervals, suggesting a relationship between DMA exposure during deposition and oxygen deficiency in the TiO_2 films. The longer purge time results in less integrated exposure of the TiO_2 film to DMA, as DMA is removed from the chamber more effectively. The calculated integrated exposure dose is 0.16 Torr·s for the TiO_2 film deposited with 120 s of N_2 purging, while the dose reduces to 0.11 Torr·s with 300 s purge duration. The integrated exposure dose was estimated as the product of the total partial pressure of DMA

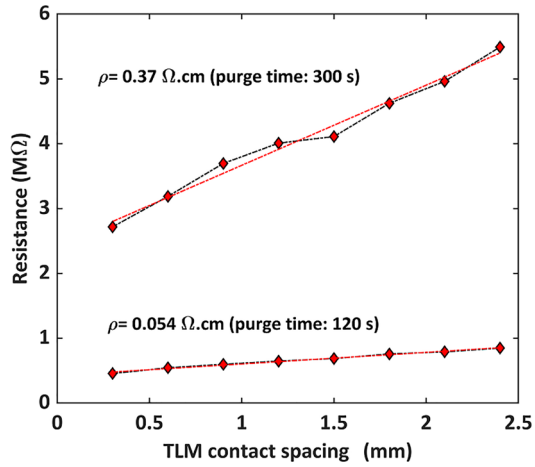

Figure 5. In-plane resistance of deposited TiO_2 films versus TLM pad spacing, which shows an increase in the resistivity for increasing purge time between each ALD half-cycle from 120 to 300 s. The measurements were performed on linear TLM test patterns with dimensions of 50 μm × 30 μm. The TiO_2 films were deposited using 240 ALD cycles of TDMAT and water vapor at a substrate temperature of 175 °C, giving the thickness of 10.1 and 7.85 nm for 120 and 300 s of N_2 purge intervals, respectively.

during one ALD cycle, the exposure duration (duration of one ALD cycle), and the frequency of exposure (number of ALD cycles). In the inert gas purge steps separating each TDMAT and H_2O dose, the dimethylamine product is removed from the chamber; however, the efficiency of this process is limited by the pumping speed, chamber design, etc. These factors are rarely reported in scientific publications, but they are very important as they may contribute to significant lab-to-lab variability in the resulting film properties already noted for as-deposited ALD-TiO_2.

To isolate the effects of DMA exposure of the films from the observed densification of the films and possible differences in incorporation of residual species in the films during their deposition for varying purge durations, annealing in dimethylamine, at the end of TiO_2 atomic layer deposition, was investigated. X-ray reflectivity data indicate that the DMA in situ annealing conditions used do not significantly alter the thickness and density of the TiO_2 films (Supporting Information, Figure S6).

Figure 6a shows a decrease in the resistivity after annealing of the ALD-TiO_2 films in DMA for 30 min. As depicted in Figure 6b, the resistance of the films monotonically decreases as DMA annealing time increases to 60 min.

X-ray photoelectron spectroscopy was used to test for evidence of reduction of the TiO_2 films as a result of DMA exposure under ALD-like conditions. The fraction of titanium ions in the Ti^{3+} oxidation state was investigated by ex situ angle-resolved XPS. Figure 7 shows XPS Ti 2p and O 1s core level spectra for a film annealed in DMA in situ in the ALD reactor for 30 min that are collected over several θ values. The angle θ is defined relative to the film surface. The surface sensitivity of the measurement is increased by tilting the sample with respect to the analyzer over θ values from 65° to 25°. Comparison of XPS data collected at θ = 25° (more surface-sensitive) to that at θ = 65° (more bulk-sensitive) for DMA-annealed TiO_2 films shows a shoulder at lower binding energy in the more bulk sensitive Ti 2p spectra (Figure 7a) at an energy corresponding to that reported for Ti^{3+}.[34−36] The θ

https://doi.org/10.1021/acs.jpclett.1c00115
J. Phys. Chem. Lett. 2021, 12, 3625−3632

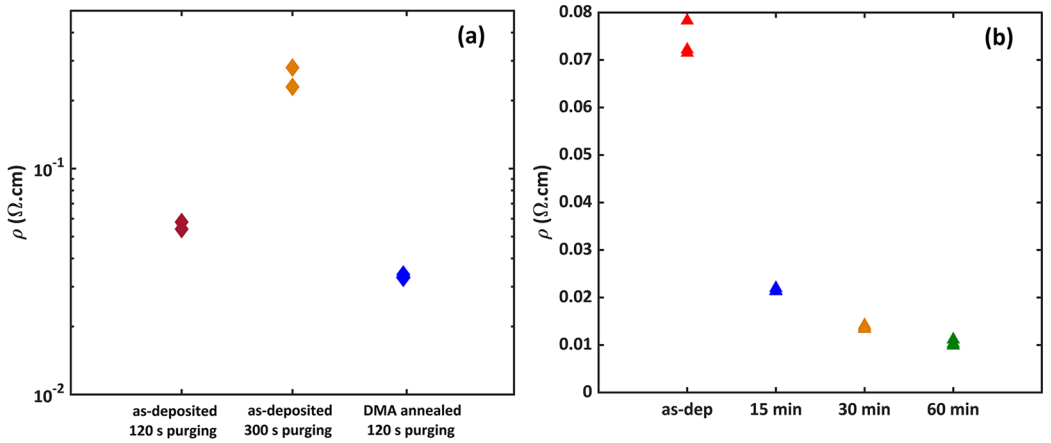

Figure 6. (a) Average resistivity of deposited TiO_2 films for different ALD conditions. The reported values show the average of four measurements across a 1 cm × 1 cm TiO_2 sample. Two TiO_2 samples were measured for each ALD condition. The as-deposited TiO_2 films were deposited using 240 ALD cycles of TDMAT and water vapor at a substrate temperature of 175 °C, using 120 and 300 s of N_2 purge intervals, respectively. (b) Transient changes in TiO_2 resistivity as a function of DMA annealing time. For each annealing condition, three measurements were taken across a 1 cm × 1 cm TiO_2 sample. The obtained resistivity values indicate that DMA has the potential to reduce the TiO_2 film transiently. Annealed TiO_2 films were prepared by in situ annealing in the ALD chamber at the end of film deposition and at the same temperature, 175 °C, in dimethylamine ambient at 1 sccm at a base pressure of ∼1−2 mTorr for 15 to 60 min. Annealed samples were deposited by 240 ALD cycles using 120 s of N_2 purge time between TDMAT and water pulses.

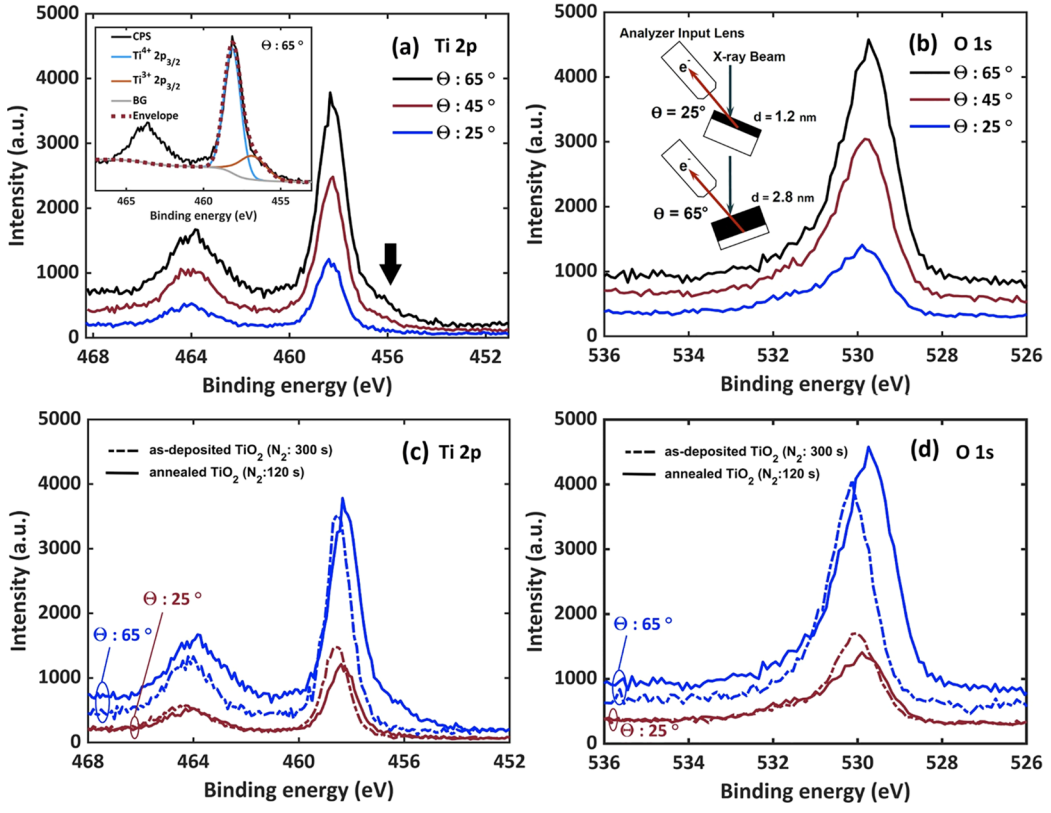

Figure 7. Angle-resolved XPS spectra: (a) Ti 2p, (b) O 1s for the TiO_2 sample annealed in DMA for 30 min. Comparison of XPS data (c) Ti 2p and (d) O 1s for DMA annealed (30 min) and as-deposited TiO_2 samples with 300 s N_2 purge time. The angle between the incident X-ray beam and the electron energy analyzer was maintained at ∼45°. Take-off angle was increased by tilting the sample with respect to the analyzer over θ values of 25°, 45°, and 65°. The angle, θ, is defined relative to the film surface.

= 25° spectrum does not exhibit this feature as strongly as the θ = 65° possibly due to reoxidation of the near-surface region during postgrowth exposure to lab atmosphere prior to sample loading in the XPS chamber. The high resolution XPS spectra for the DMA-annealed samples in Figure 7c show the Ti 2p doublet, Ti $2p_{3/2}$ at binding energy of 458.3 eV and Ti $2p_{1/2}$ at 464 eV, arising from spin orbit splitting. These peaks are consistent with Ti^{4+} in TiO_2.[37,38] Fitting of the Ti $2p_{3/2}$ peak showed a significant low binding energy shoulder associated with Ti^{3+} after annealing. The area attributed to the Ti^{3+} peak increases by 18% in the DMA-annealed sample in the more bulk sensitive Ti 2p spectra. Peak fitting was performed using

https://doi.org/10.1021/acs.jpclett.1c00115
J. Phys. Chem. Lett. 2021, 12, 3625−3632

Ti^{4+} at 458.6 eV and Ti^{3+} at 456.7 eV (Figure 7a, inset). This is consistent with the 1.7−1.9 eV shift that has been reported in binding energy for photoemission associated with Ti^{3+} relative to the main emission line of Ti^{4+}.[36,39,40] In contrast, the as-deposited TiO_2 film deposited with longer purging time, 300 s, does not exhibit the lower binding energy shoulder, consistent with negligible Ti^{3+} photoemission. Relative contributions of the Ti^{3+} oxidation state to the measured Ti $2p_{3/2}$ features, as estimated from peak fitting, are summarized in Table 1. The

Table 1. $Ti^{3+}/(Ti^{3+} + Ti^{4+})$ Peak Area Ratio in Percentage Obtained from Ti 2p3/2 Peak Fitting for As-Deposited and Annealed Ti 2p Spectra at Different Take-off Angles[a]

	θ = 65°	θ = 25°
as-deposited TiO_2 (N_2 purge: 300 s)	0.02	0
as-deposited TiO_2 (N_2 purge: 120 s)	5.1	4.3
annealed TiO_2 (N_2 purge: 120 s)	22.7	8.1

[a]More information on the XPS fittings can be found in Figure S9 of the Supporting Information.

Ti^{3+} peak area increases significantly after DMA-annealing under the ALD-like conditions employed in these experiments. As-deposited TiO_2 for which a 120 s purge was used in the ALD process exhibits a relative Ti^{3+} peak area intermediate between that of the DMA-annealed film and the as-deposited/300 s sample. This indicates an intermediate level of effective electron doping of the films prepared using this purge condition, consistent with the measured resistance and sheet resistivity values in Figures 5 and 6. The XPS Ti 2p core level spectra for the three different samples shown in Table 1 (DMA-annealed, and unannealed for two different purge durations) are provided in Figure S8.

We observe ∼0.3 eV higher binding energy values for the as-deposited TiO_2 spectra compared to the DMA-annealed case in the Ti 2p spectra collected at θ = 65°. A similar shift of ∼0.4 eV is observed in the oxygen O 1s spectra (Figure 7d). In Figure 7, all peak positions were referenced to C 1s at 284.8 eV to compensate for the possible effects of charging during the measurement; therefore, charging cannot account for the differences in core level binding energies observed in Figure 7c and d. Instead, the higher binding energies of the Ti 2p and O 1s core level features detected at θ = 65° may indicate near-surface band-bending in the unannealed films. Such band bending can result from the presence of negatively charged TiO_2 surface states. Negative charge originating from surface and near-surface defects that produce states within the band gap of TiO_2[33,34] may cause a surface potential barrier for photoelectrons emitted from the bulk of the ALD-grown film, a barrier that is lowered after DMA annealing increases the bulk oxygen deficiency[41,42] and effectively dopes the film n-type. This hypothesis is consistent with the much reduced binding energy difference for unannealed versus DMA annealed films observed in the more surface-sensitive θ = 25° spectra of Figure 7c and d.

Observation of Ti^{3+} is consistent with reports of oxygen vacancies acting as donor defects in TiO_2, providing electron doping of the titanium oxide film.[43] Electrons trapped at titanium ions in the oxide provide enhanced electronic conduction via polaron hopping.[44] Oxygen defects and Ti^{3+} sites dominate the physical and chemical properties in TiO_2,[45−48] with reports of near-surface vacancy concentrations being modified by dosing of oxygen and nitrogen.[49,50] XPS analyses of the as-deposited (both purge times) and DMA annealed samples prepared in the current experiments do not detect either nitrogen or carbon impurities, species that may affect the electrical conductivity of the ALD-TiO_2 films if they are incorporated at a sufficiently high concentration (Supporting Information, Figure S7).

Nunez et al. demonstrated that the concentration of Ti^{3+} in the amorphous ALD-TiO_2 thin films they studied was directly correlated with the electronic conductivity for different precursor chemistries and deposition temperatures. The authors detected a defect band in the TiO_2 band gap by photoelectron spectroscopy and a strong Ti^{3+} signal in electron paramagnetic (EPR) signal, supporting the assignment of the defect peak in their XPS valence band spectra to localized Ti^{3+} sites.[51] The defect band emission and the obtained EPR signal were much stronger for TDMAT-derived ALD-TiO_2 films compared to those derived from $TiCl_4$ precursor. This difference in behavior may result from DMA exposure during the TDMAT ALD process, as reported herein.

DMA exposure increases the conductivity of ALD-TiO_2 by reducing the film, increasing the effective n-type doping and introducing Ti^{3+} states. In agreement with this picture, TiO_2 thin films deposited by dc magnetron sputtering[52] have recently been observed to act as effective solid-state sensors for DMA. This was attributed to a reduction reaction produced by exposure of the metal oxide surface to DMA molecules, enhancing the surface electronic conductivity.[52,53]

Our findings emphasize the importance of in situ monitoring of gas phase chemistry to achieve well-controlled functional properties in ALD-grown metal oxide thin films. Similar redox reactions involving gas phase ALD products or intermediate species may alter the stoichiometry and properties of metal oxide films in other materials systems beyond TiO_2.

Real-time residual gas analysis provides a link between changes in gas phase chemistry during ALD half-cycle reactions and the electrical conductivity of TiO_2 films. Production of DMA vapor was probed for both the TDMAT and water vapor half-reactions during the TDMAT/H_2O ALD process. The extent of film exposure to DMA, a reducing agent, in the ALD chamber throughout each reaction half-cycle was correlated with both an increase in the ALD TiO_2 electronic conductivity, and the observation of Ti^{3+} oxidation state by ex situ X-ray photoelectron spectroscopy analysis. Understanding the DMA-induced reduction of ALD-TiO_2 described herein may facilitate the control of electronic conductivity and other important properties of ALD-grown TiO_2 thin films and provides lessons for other ALD reaction chemistries and thin film materials systems.

■ ASSOCIATED CONTENT

Supporting Information

The Supporting Information is available free of charge at https://pubs.acs.org/doi/10.1021/acs.jpclett.1c00115.

Description of RGA system and detailed methods and analysis for XRR and XPS (PDF)

■ AUTHOR INFORMATION

Corresponding Author

Paul C. McIntyre − *Department of Materials Science & Engineering, Stanford University, Stanford, California 94305, United States*; Email: pcm1@slac.stanford.edu

https://doi.org/10.1021/acs.jpclett.1c00115
J. Phys. Chem. Lett. 2021, 12, 3625−3632

Authors

Aein S. Babadi − *Department of Materials Science & Engineering, Stanford University, Stanford, California 94305, United States;* orcid.org/0000-0002-6626-6560

Robert Tang-Kong − *Department of Materials Science & Engineering, Stanford University, Stanford, California 94305, United States;* orcid.org/0000-0003-4583-460X

Complete contact information is available at: https://pubs.acs.org/10.1021/acs.jpclett.1c00115

Notes

The authors declare no competing financial interest.

■ ACKNOWLEDGMENTS

Part of this work was performed at the Stanford Nano Shared Facilities (SNSF). The authors would like to thank Prof. Piero Pianetta and Dr. Juliet Jamtgaard for guidance with XPS and Dr. Arturas Vailionis for guidance with GIXRD measurements. The authors gratefully acknowledge the financial support of the National Science Foundation Award No. CBET-1805084. We gratefully acknowledge support from Knut and Alice Wallenberg foundation.

■ REFERENCES

(1) Mistry, K.; Allen, C.; Auth, C.; Beattie, B.; Bergstrom, D.; Bost, M.; Brazier, M.; Buehler, M.; Cappellani, A.; Chau, R. A 45nm logic technology with high-k+metal gate transistors, strained silicon, 9 Cu interconnect layers, 193nm dry patterning, and 100% Pb-free packaging. *International Electron Devices Meeting*; IEEE, 2007; pp 247−250.

(2) Cho, H.-J.; Seo, K.-I.; Jeong, W.; Kim, Y.-H.; Lim, Y.; Jang, W.; Hong, J.; Suk, S.; Li, M.; Ryou, C. Bulk planar 20nm high-k/metal gate CMOS technology platform for low power and high performance applications. *International Electron Devices Meeting*; IEEE, 2011; pp 15.1.1−15.1.4.

(3) Chen, Y. W.; Prange, J. D.; Dühnen, S.; Park, Y.; Gunji, M.; Chidsey, C. E. D.; McIntyre, P. C. Atomic layer-deposited tunnel oxide stabilizes silicon photoanodes for water oxidation. *Nat. Mater.* **2011**, *10* (7), 539−544.

(4) Abdulagatov, A. I.; Yan, Y.; Cooper, J. R.; Zhang, Y.; Gibbs, Z. M.; Cavanagh, A. S.; Yang, R. G.; Lee, Y. C.; George, S. M. Al_2O_3 and TiO_2 atomic layer deposition on copper for water corrosion resistance. *ACS Appl. Mater. Interfaces* **2011**, *3* (12), 4593−601.

(5) O'Neill, B. J.; Jackson, D. H. K.; Lee, J.; Canlas, C.; Stair, P. C.; Marshall, C. L.; Elam, J. W.; Kuech, T. F.; Dumesic, J. A.; Huber, G. W. Catalyst Design with Atomic Layer Deposition. *ACS Catal.* **2015**, *5* (3), 1804−1825.

(6) Hendricks, O. L.; Tang-Kong, R.; Babadi, A. S.; McIntyre, P. C.; Chidsey, C. E. D. Atomic Layer Deposited TiO_2−IrO_x Alloys Enable Corrosion Resistant Water Oxidation on Silicon at High Photovoltage. *Chem. Mater.* **2019**, *31* (1), 90−100.

(7) Memarzadeh Lotfabad, E.; Kalisvaart, P.; Cui, K.; Kohandehghan, A.; Kupsta, M.; Olsen, B.; Mitlin, D. ALD TiO_2 coated silicon nanowires for lithium ion battery anodes with enhanced cycling stability and coulombic efficiency. *Phys. Chem. Chem. Phys.* **2013**, *15* (32), 13646−57.

(8) Wise, A. M.; Ban, C.; Weker, J. N.; Misra, S.; Cavanagh, A. S.; Wu, Z.; Li, Z.; Whittingham, M. S.; Xu, K.; George, S. M.; Toney, M. F. Effect of Al_2O_3 Coating on Stabilizing $LiNi_{0.4}Mn_{0.4}Co_{0.2}O_2$ Cathodes. *Chem. Mater.* **2015**, *27* (17), 6146−6154.

(9) Han, X.; Liu, Y.; Jia, Z.; Chen, Y. C.; Wan, J.; Weadock, N.; Gaskell, K. J.; Li, T.; Hu, L. Atomic-layer-deposition oxide nanoglue for sodium ion batteries. *Nano Lett.* **2014**, *14* (1), 139−47.

(10) Melskens, J.; van de Loo, B. W.; Macco, B.; Black, L. E.; Smit, S.; Kessels, W. Passivating contacts for crystalline silicon solar cells: From concepts and materials to prospects. *IEEE Journal of Photovoltaics* **2018**, *8* (2), 373−388.

(11) Black, L.; Van De Loo, B.; Macco, B.; Melskens, J.; Berghuis, W.; Kessels, W. Explorative studies of novel silicon surface passivation materials: Considerations and lessons learned. *Sol. Energy Mater. Sol. Cells* **2018**, *188*, 182−189.

(12) Mikulik, D.; Meng, A. C.; Berrazouane, R.; Stückelberger, J.; Romero-Gomez, P.; Tang, K.; Haug, F.-J.; Fontcuberta i Morral, A.; McIntyre, P. C. Surface Defect Passivation of Silicon Micropillars. *Adv. Mater. Interfaces* **2018**, *5* (20), 1800865.

(13) Bonilla, R. S.; Hoex, B.; Hamer, P.; Wilshaw, P. R. Dielectric surface passivation for silicon solar cells: A review. *Phys. Status Solidi A* **2017**, *214* (7), 1700293.

(14) Hoex, B.; Heil, S. B. S.; Langereis, E.; van de Sanden, M. C. M.; Kessels, W. M. M. Ultralow surface recombination of c-Si substrates passivated by plasma-assisted atomic layer deposited Al_2O_3. *Appl. Phys. Lett.* **2006**, *89* (4), 042112.

(15) Banerjee, S.; Dionysiou, D. D.; Pillai, S. C. Self-cleaning applications of TiO_2 by photo-induced hydrophilicity and photocatalysis. *Appl. Catal., B* **2015**, *176*−*177*, 396−428.

(16) Hashimoto, K.; Irie, H.; Fujishima, A. TiO_2 Photocatalysis: A Historical Overview and Future Prospects. *Jpn. J. Appl. Phys.* **2005**, *44* (12), 8269−8285.

(17) Lan, Y.; Lu, Y.; Ren, Z. Mini review on photocatalysis of titanium dioxide nanoparticles and their solar applications. *Nano Energy* **2013**, *2* (5), 1031−1045.

(18) Nagamatsu, K. A.; Avasthi, S.; Sahasrabudhe, G.; Man, G.; Jhaveri, J.; Berg, A. H.; Schwartz, J.; Kahn, A.; Wagner, S.; Sturm, J. C. Titanium dioxide/silicon hole-blocking selective contact to enable double-heterojunction crystalline silicon-based solar cell. *Appl. Phys. Lett.* **2015**, *106* (12), 123906.

(19) Yin, X.; Battaglia, C.; Lin, Y.; Chen, K.; Hettick, M.; Zheng, M.; Chen, C.-Y.; Kiriya, D.; Javey, A. 19.2% Efficient InP heterojunction solar cell with electron-selective TiO_2 contact. *ACS Photonics* **2014**, *1* (12), 1245−1250.

(20) Yang, X.; Bi, Q.; Ali, H.; Davis, K.; Schoenfeld, W. V.; Weber, K. High-Performance TiO_2-Based Electron-Selective Contacts for Crystalline Silicon Solar Cells. *Adv. Mater.* **2016**, *28* (28), 5891−5897.

(21) Tan, W.; Bowring, A. R.; Babadi, A. S.; Meng, A. C.; Tang-Kong, R.; McGehee, M. D.; McIntyre, P. C. Interfacing Low-Temperature Atomic Layer Deposited TiO_2 Electron Transport Layers with Metal Electrodes. *Adv. Mater. Interfaces* **2020**, *7* (8), 1902054.

(22) Tang-Kong, R.; Winter, R.; Brock, R.; Tracy, J.; Eizenberg, M.; Dauskardt, R. H.; McIntyre, P. C. The Role of Catalyst Adhesion in ALD-TiO_2 Protection of Water Splitting Silicon Anodes. *ACS Appl. Mater. Interfaces* **2018**, *10* (43), 37103−37109.

(23) Scheuermann, A. G.; et al. Titanium Oxide Crystallization and Interface Defect Passivation for High Performance Insulator-Protected Schottky Junction MIS Photoanodes. *ACS Appl. Mater. Interfaces* **2016**, *8* (23), 14596−603.

(24) Scheuermann, A. G.; Prange, J. D.; Gunji, M.; Chidsey, C. E.; McIntyre, P. C. Effects of catalyst material and atomic layer deposited TiO_2 oxide thickness on the water oxidation performance of metal−insulator−silicon anodes. *Energy Environ. Sci.* **2013**, *6* (8), 2487−2496.

(25) Hu, S.; et al. Amorphous TiO_2 coatings stabilize Si, GaAs, and GaP photoanodes for efficient water oxidation. *Science* **2014**, *344* (6187), 1005−1009.

(26) Atkinson, R.; et al. Kinetics and mechanisms of the gas-phase reactions of ozone with organic compounds under atmospheric conditions. *Chem. Rev.* **1984**, *84* (5), 437−470.

(27) Widjaja, Y.; Musgrave, C. B. Quantum chemical study of the mechanism of aluminum oxide atomic layer deposition. *Appl. Phys. Lett.* **2002**, *80* (18), 3304−3306.

(28) Naldoni, A.; Allieta, M.; Santangelo, S.; Marelli, M.; Fabbri, F.; Cappelli, S.; Bianchi, C. L.; Psaro, R.; Dal Santo, V. Effect of Nature

and Location of Defects on Bandgap Narrowing in Black TiO_2 Nanoparticles. *J. Am. Chem. Soc.* **2012**, *134* (18), 7600−7603.
(29) Gordon, R. G.; Hausmann, D.; Kim, E.; Shepard, J. A kinetic model for step coverage by atomic layer deposition in narrow holes or trenches. *Chem. Vap. Deposition* **2003**, *9* (2), 73−78.
(30) Okada, L.; et al. Adsorption and desorption kinetics of tetrakis (dimethylamino) titanium and dimethylamine on TiN surfaces. *Appl. Surf. Sci.* **1999**, *137* (1−4), 113−124.
(31) Shang, Y.; et al. Chemical kinetics of H-abstractions from dimethyl amine by H, CH_3, OH, and HO_2 radicals with multi-structural torsional anharmonicity. *Phys. Chem. Chem. Phys.* **2019**, *21* (23), 12685−12696.
(32) Slagle, I. R.; Dudich, J. F.; Gutman, D. Direct identification of reactive routes in the reaction of oxygen atoms with dimethylamine. *Chem. Phys. Lett.* **1979**, *61* (3), 620−624.
(33) Sønsteby, H. H.; Yanguas-Gil, A.; Elam, J. W. Consistency and reproducibility in atomic layer deposition. *J. Vac. Sci. Technol., A* **2020**, *38* (2), 020804.
(34) Pan, J. M.; et al. Interaction of water, oxygen, and hydrogen with TiO_2(110) surfaces having different defect densities. *J. Vac. Sci. Technol., A* **1992**, *10* (4), 2470−2476.
(35) Henkel, K.; et al. In-gap states in titanium dioxide and oxynitride atomic layer deposited films. *J. Vac. Sci. Technol., A* **2017**, *35* (1), 01B135.
(36) Jackman, M. J.; Thomas, A. G.; Muryn, C. Photoelectron spectroscopy study of stoichiometric and reduced anatase TiO_2 (101) surfaces: the effect of subsurface defects on water adsorption at near-ambient pressures. *J. Phys. Chem. C* **2015**, *119* (24), 13682−13690.
(37) Sanjinés, R.; Tang, H.; Berger, H.; Gozzo, F.; Margaritondo, G.; Lévy, F. Electronic structure of anatase TiO_2 oxide. *J. Appl. Phys.* **1994**, *75* (6), 2945−2951.
(38) Diebold, U.; Madey, T. E. TiO_2 by XPS. *Surf. Sci. Spectra* **1996**, *4* (3), 227−231.
(39) Biesinger, M. C.; Lau, L. W. M.; Gerson, A. R.; Smart, R. S. C. Resolving surface chemical states in XPS analysis of first row transition metals, oxides and hydroxides: Sc, Ti, V, Cu and Zn. *Appl. Surf. Sci.* **2010**, *257* (3), 887−898.
(40) Kashiwaya, S.; Morasch, J.; Streibel, V.; Toupance, T.; Jaegermann, W.; Klein, A. The work function of TiO_2. *Surfaces* **2018**, *1* (1), 73−89.
(41) Wendt, S.; Sprunger, P. T.; Lira, E.; Madsen, G. K. H.; Li, Z.; Hansen, J. Ø.; Matthiesen, J.; Blekinge-Rasmussen, A.; Lægsgaard, E.; Hammer, B.; Besenbacher, F. The Role of Interstitial Sites in the Ti3d Defect State in the Band Gap of Titania. *Science* **2008**, *320* (5884), 1755−1759.
(42) Morita, K.; Shibuya, T.; Yasuoka, K. Stability of Excess Electrons Introduced by Ti Interstitial in Rutile TiO_2(110) Surface. *J. Phys. Chem. C* **2017**, *121* (3), 1602−1607.
(43) Di Valentin, C.; Pacchioni, G.; Selloni, A. Reduced and n-Type Doped TiO_2: Nature of Ti^{3+} Species. *J. Phys. Chem. C* **2009**, *113* (48), 20543−20552.
(44) Pham, H. H.; Wang, L.-W. Oxygen vacancy and hole conduction in amorphous TiO_2. *Phys. Chem. Chem. Phys.* **2015**, *17* (1), 541−550.
(45) Deskins, N. A.; Rousseau, R.; Dupuis, M. Distribution of Ti^{3+} surface sites in reduced TiO_2. *J. Phys. Chem. C* **2011**, *115* (15), 7562−7572.
(46) Park, S.-J.; Lee, J.-P.; Jang, J. S.; Rhu, H.; Yu, H.; You, B. Y.; Kim, C. S.; Kim, K. J.; Cho, Y. J.; Baik, S.; et al. In situ control of oxygen vacancies in TiO_2 by atomic layer deposition for resistive switching devices. *Nanotechnology* **2013**, *24* (29), 295202.
(47) Xia, T.; Zhang, Y.; Murowchick, J.; Chen, X. Vacuum-treated titanium dioxide nanocrystals: Optical properties, surface disorder, oxygen vacancy, and photocatalytic activities. *Catal. Today* **2014**, *225*, 2−9.
(48) Deskins, N. A.; Dupuis, M. Electron transport via polaron hopping in bulk TiO_2: A density functional theory characterization. *Phys. Rev. B: Condens. Matter Mater. Phys.* **2007**, *75* (19), 195212.
(49) Zuo, F.; Wang, L.; Wu, T.; Zhang, Z.; Borchardt, D.; Feng, P. Self-doped Ti^{3+} enhanced photocatalyst for hydrogen production under visible light. *J. Am. Chem. Soc.* **2010**, *132* (34), 11856−11857.
(50) Li, M.; Hebenstreit, W.; Diebold, U.; Tyryshkin, A. M.; Bowman, M. K.; Dunham, G. G.; Henderson, M. A. The influence of the bulk reduction state on the surface structure and morphology of rutile TiO_2 (110) single crystals. *J. Phys. Chem. B* **2000**, *104* (20), 4944−4950.
(51) Nunez, P.; Richter, M. H.; Piercy, B. D.; Roske, C. W.; Cabán-Acevedo, M.; Losego, M. D.; Konezny, S. J.; Fermin, D. J.; Hu, S.; Brunschwig, B. S.; Lewis, N. S. Characterization of Electronic Transport through Amorphous TiO_2 Produced by Atomic Layer Deposition. *J. Phys. Chem. C* **2019**, *123* (33), 20116−20129.
(52) Ganesan, S.; Muruganandham, A.; Mounasamy, V.; Kannan, V. P.; Madanagurusamy, S. Highly Selective Dimethylamine Sensing Performance of TiO_2 Thin Films at Room Temperature. *J. Nanosci. Nanotechnol.* **2020**, *20* (5), 3131−3139.
(53) Takao, Y.; Nakanishi, M.; Kawaguchi, T.; Shimizu, Y.; Egashira, M. Semiconductor dimethylamine gas sensors with high sensitivity and selectivity. *Sens. Actuators, B* **1995**, *25* (1), 375−379.

https://doi.org/10.1021/acs.jpclett.1c00115
J. Phys. Chem. Lett. 2021, 12, 3625−3632